Reduced order model of nonlinear structures for turbomachinery aeroelasticity

Théo Flament, Jean-François Deü, Antoine Placzek, Mikel Balmaseda, Duc-Minh Tran

REDUCED ORDER MODEL OF NONLINEAR STRUCTURES FOR TURBOMACHINERY AEROELASTICITY

T. Flament[1,2,†,*], J-F. Deü[2], A. Placzek[1], M. Balmaseda[3], D-M. Tran[4],

[1]DAAA, ONERA, Université Paris Saclay F-92322 Châtillon - France
[2]LMSSC, Cnam, HESAM Université, F-75003 Paris, France
[3]DAAA, ONERA, Université Paris Saclay F-92190 Meudon - France
[4]DMAS, ONERA, Université Paris Saclay F-92322 Châtillon - France

ABSTRACT

This work concerns the numerical modeling of geometric nonlinear vibrations of slender structures in rotation using an original reduced order model based on the use of dual modes along with the implicit condensation method. This approach is an improvement of the classical ICE method in the sense that the membrane stretching effect is taken into account in the dynamic resolution. The dynamics equations are firstly presented and the construction of the reduced order model (ROM) is then proposed. The second part of the paper deals with numerical applications using the finite element method, first for a 3D cantilever beam, then for an Ultra High Bypass Ratio (UHBR) fan blade. In the applications considered, the proposed method predicts more accurately the geometrically nonlinear behavior than the ICE method.

Keywords: Structural dynamics, vibration, geometric nonlinearity, nonlinear model order reduction, fluid-structure interaction, aeroelasticity

NOMENCLATURE

Acronyms

CFD	Computational Fluid Dynamics
CSM	Computational Structural Dynamics
FE	Finite Elements
FOM	Full Order model
IC	Implicit Condensation
ICE	Implicit Condensation and Expansion
ICDual	Implicit Condensation with a reduction basis containing linear normal modes and dual modes
ROM	Reduced Order Model
SVD	Singular Value Decomposition
UHBR	Ultra High Bypass Ratio

Symbols

$\mathbf{d}_i$	i^{th} mode resulting from the SVD
$\mathbf{D}$	Basis of the dual modes
$\mathscr{E}_i$	Linearized strain energy contribution of the SVD mode i
$\mathbf{f_{nl}}$	Internal geometrical nonlinear forces
$\mathbf{f_{ext}}$	External forces applied to the structure
$\mathbf{f}_k$	External static forces applied to the structure for the construction of the ICE and ICDual models
$\mathbf{g_{nl}}$	Internal geometrical nonlinear forces of the centrifugally prestressed structure
$\widetilde{g}_{nl}^{\,k}$	Projection of $\mathbf{g_{nl}}$ on the k^{th} linear mode
$\mathbf{K}$, $\mathbf{M}$, $\mathbf{C}$	Elastic stiffness, mass and viscous damping matrices
$\mathbf{K_c}$	Centrifugal softening stiffness matrix
$\mathbf{K_{nl}}(\mathbf{u_s})$	Tangent stiffness matrix at the prestressed position
$\mathbf{K}(\Omega)$	Total stiffness of the structure
$\widetilde{\mathbf{K}}$, $\widetilde{\mathbf{M}}$, $\widetilde{\mathbf{C}}$	Reduced stiffness, mass and damping matrices
$\mathbf{q}$	Generalized coordinates
$\mathbf{r}_k$	Residual of the k^{th} static solution
$\mathbf{u}$, $\dot{\mathbf{u}}$, $\ddot{\mathbf{u}}$	Displacements, velocity, acceleration
$\mathbf{u_{ICE}}$	Rebuilt displacement obtained with the ICE method
$\mathbf{u_s}$	Prestressed displacement of the structure under centrifugal forces
$\mathbf{u_t}$	Total displacement $\mathbf{u} + \mathbf{u_s}$
$\mathbf{V}$	Reduction basis
α_{HHT}	Coefficient of the HHT-α method
Ω	Rotation speed around the fixed axis
$\mathbf{\Phi}^{\Omega}$	Matrix of the linear normal modes of the centrifugally prestressed structure
$\boldsymbol{\phi}_i^{\Omega}$	i^{th} linear normal modes in the basis $\mathbf{\Phi}^{\Omega}$
ω_i	Pulsation of the i^{th} linear normal mode
$\mathbf{\Psi}$	Reconstruction modes for the *Expansion* step of the ICE method
$\boldsymbol{\eta}$	Generalized coordinates associated to $\mathbf{\Psi}$
ξ	Damping coefficient: $\mathbf{C} = 2\xi\omega_0\mathbf{M}$

[†]Joint first authors
[*]Corresponding author: theo.flament@onera.fr
Documentation for `asmeconf.cls`: Version 1.32, April 7, 2023.

1. INTRODUCTION

Performance optimization for the next generation of aircraft engines leads to propellers and blades of large dimensions. Such structures are more flexible and may be subjected to large amplitudes of vibrations, hence triggering geometric nonlinearities that alter the levels of vibration and have an impact on aeroelastic phenomena such as flutter or forced response. To characterize the aeroelastic phenomena, a usual method is to use a partitioned procedure involving a dedicated CFD solver for the fluid and a CSM solver for the structure. However, such a coupling has two major limitations. First, the resulting computational time is prohibitive for industrial applications, and second, the coupling between the two solvers is tedious in terms of transfer of information. To overcome these limitations, an efficient method is to perform the partitioned coupling between a CFD solver to keep the high fidelity for the fluid, and a reduced-order model (ROM) for the structure. The latter is built in a way to be independent of a CSM solver, giving the possibility to change the fluid solver with another. In the literature, several methods are available for building reduced-order models taking into account structural geometric nonlinearities. An approach is the projection on a reduction basis containing both the first linear normal modes of the structure and additional modes aimed at capturing the nonlinearity, such as modal derivatives [1, 2] or dual modes [3–5]. This method is non-intrusive and flexible but the difficulty relies on the determination of the additional modes. Another approach is the use of invariant manifolds [6, 7] adapted to periodic vibrations in the vicinity of linear normal modes. Nevertheless, this method is intrusive when high precision is desired, meaning that it is necessary to have access to specific information inside a FE solver, which is not the case for industrial CSM solvers. The same intrusive limitation is encountered for hyper-reduction methods such as the Discrete Empirical Interpolation Method (DEIM) [8] for which the nonlinearity is computed only at a few degrees of freedom. Other methods are based on the results of previous high-fidelity computations such as the Proper Orthogonal Decomposition (POD) method [9–11]. However, the preliminary computations required to determine the projection basis are computationally expensive and are case-dependent for the given set of parameters.

In this paper, the ROM is built by projection on a reduction basis including linear normal modes and additional dual modes. The internal geometric nonlinear forces are approximated as a third-order polynomial of the generalized coordinates with coefficients identified using the *Implicit Condensation* (IC) method [12]. In the literature, the IC method involves only the bending modes, and an *Expansion* step (ICE) [13] is commonly introduced to post-process the in-plane dynamics. This post-processing step may be viewed as a static compensation. The limitation is that the in-plane dynamics is only rebuilt and not taken into account in the resolution of the reduced equation of the dynamics. The literature suggests an *inertial compensation* [14] to take into account the in-plane dynamics into the equations relative to the bending modes. This modification changes the nature of the equation that becomes less convenient to integrate. Such a method was recently enhanced by a *Force Compensation* [15] in order to tackle following forces. In the present paper we choose to add dual modes to the reduction basis in order to compute the in-plane dynamics directly in the reduced equations of the motion. The *Expansion* step of the ICE method is therefore no longer needed and the nature of the reduced equation of the dynamics remains unchanged. This method has already been applied by the authors on a 2D case in the frame of a fluid-structure interaction between the vortex shedding in the wake of a fixed cylinder and a von Kármán beam [16]. In this paper the method is used for 3D finite element structures subjected to rotation around a fixed axis.

The first part of this paper deals with the structural dynamics modeling and the construction of the nonlinear reduced-order model (ROM). Then the interest of such a ROM is shown on 3D structures in rotation with the example of a cantilever beam-like 3D test case and a fan blade. The selection of the dual modes is detailed along with the determination of the nonlinear coefficients of the internal forces. The precision of the ROM is checked and its robustness discussed. Finally, preliminary applications to a fan blade are described.

2. STRUCTURAL DYNAMICS EQUATIONS

The finite element discretization of the structure is considered as the reference full-order model (FOM). The vibration of the structure verifies the following matrix equation:

$$\mathbf{M}\ddot{\mathbf{u}} + \mathbf{C}\dot{\mathbf{u}} + \mathbf{K}\mathbf{u} + \mathbf{f_{nl}}(\mathbf{u}) = \mathbf{f_{ext}}(t), \tag{1}$$

with $\mathbf{u}$ the displacement degrees of freedom vector, $\mathbf{M}$ the mass matrix, $\mathbf{C}$ the damping matrix and $\mathbf{K}$ the stiffness matrix. The damping model is the widely used Rayleigh viscous damping: $\mathbf{C} = \alpha\mathbf{M} + \beta\mathbf{K}$. Moreover, $\mathbf{f_{nl}}$ is the vector of the internal geometrical nonlinear forces and $\mathbf{f_{ext}}(t)$ is the external force applied to the structure, which may depend on the position and the velocity of the structure, like aerodynamic forces for instance.

When turbomachines or propellers are considered, the structure is in rotation around a fixed axis and centrifugal effects contribute to the dynamics. The rotation speed around its axis is considered constant and the total displacement degrees of freedom of the structure, defined as $\mathbf{u}$ in Eq.(1), are now written $\mathbf{u_t}$. The total displacement is the sum of a static nonlinear displacement $\mathbf{u_s}$ due to the centrifugal external force, and of vibrations $\mathbf{u}$ around this prestressed position: $\mathbf{u_t} = \mathbf{u_s} + \mathbf{u}$. The prestressed position $\mathbf{u_s}$ is solution of:

$$(\mathbf{K} - \mathbf{K_c})\mathbf{u_s} + \mathbf{f_{nl}}(\mathbf{u_s}) = \mathbf{f^{\Omega}}. \tag{2}$$

Centrifugal effects are included in the softening matrix $\mathbf{K_c}$ and the constant centrifugal load $\mathbf{f^{\Omega}}$. The geometric nonlinearities $\mathbf{f_{nl}}$ are expanded around the prestressed solution $\mathbf{u_s}$:

$$\mathbf{f_{nl}}(\mathbf{u_s} + \mathbf{u}) = \mathbf{f_{nl}}(\mathbf{u_s}) + \mathbf{K_{nl}}(\mathbf{u_s})\mathbf{u} + \mathbf{g_{nl}}(\mathbf{u}), \tag{3}$$

where $\mathbf{K_{nl}}(\mathbf{u_s})$ is the tangent stiffness matrix, i.e. the Jacobian of $\mathbf{f_{nl}}(\mathbf{u_t})$ evaluated at the prestressed position $\mathbf{u_s}$, and $\mathbf{g_{nl}}(\mathbf{u})$ is the vector of the nonlinear forces with respect to the prestressed position. In the rotating frame, the equation governing the vibrations of the structure around the centrifugally prestressed position is:

$$\mathbf{M}\ddot{\mathbf{u}} + \mathbf{C}\dot{\mathbf{u}} + \underbrace{\left[\mathbf{K} - \mathbf{K_c} + \mathbf{K_{nl}}(\mathbf{u_s})\right]}_{\mathbf{K}(\Omega)}\mathbf{u} + \mathbf{g_{nl}}(\mathbf{u}) = \mathbf{f_{ext}}(t), \tag{4}$$

in which the gyroscopic effect was neglected. Due to the centrifugal and geometrical nonlinear effects, a hardening or softening behavior can be observed depending on the speed of rotation and the considered mode [17].

External forces imposed to the structure in the test cases considered in this paper are independent from the position. Future work will involve external forces corresponding to aerodynamic loads depending on the position and velocity of the structure $\mathbf{f_{ext}}(\mathbf{u_s}+\mathbf{u}, \dot{\mathbf{u}})$.

3. REDUCED-ORDER MODELS BY PROJECTION

Equation (4) involves a large number of degrees of freedom when industrial models are considered. Projection-based reduced order models rely on the assumption that the degrees of freedom $\mathbf{u}$ can be approximated by a limited combination of vectors (later called modes). These vectors form a basis of reduced dimension $\mathbf{V}$ such that $\mathbf{u} \approx \mathbf{Vq}$. The linear normal modes of the structure are usually considered for this reduction basis; they are solutions to the following eigenvalue problem:

$$\mathbf{K}(\Omega)\boldsymbol{\phi}_i^{\Omega} = \omega_i^2(\Omega)\mathbf{M}\boldsymbol{\phi}_i^{\Omega}. \tag{5}$$

Such modes are computed around the prestressed position and thus depend on the rotation speed. Only the first linear normal modes are kept in the reduction basis. For linear problems, this method is very efficient. However, the geometric nonlinearity leads to a coupling between the modes. Thus, a reduction basis containing only the first linear normal modes is not rich enough to capture the nonlinear displacements, unless a large number of modes, almost all, are used. Therefore other "modes" have to be added to the reduction basis in order to capture the nonlinearity. This topic is addressed in section 3.1.

Once the reduction basis is built, the reduced equation of the dynamics is obtained by projecting Eq.(4) on the basis of reduced dimension $\mathbf{V}$, leading to a system with only few degrees of freedom called the generalized coordinates $\mathbf{q}$:

$$\widetilde{\mathbf{M}}\ddot{\mathbf{q}} + \widetilde{\mathbf{C}}\dot{\mathbf{q}} + \widetilde{\mathbf{K}}\mathbf{q} + \mathbf{V}^T\mathbf{g_{nl}}(\mathbf{Vq}) = \mathbf{V}^T\mathbf{f_{ext}}(t), \tag{6}$$

with $\widetilde{\mathbf{M}} = \mathbf{V}^T\mathbf{MV}$, $\widetilde{\mathbf{C}} = \mathbf{V}^T\mathbf{CV}$ and $\widetilde{\mathbf{K}} = \mathbf{V}^T\mathbf{K}(\Omega)\mathbf{V}$ respectively the reduced mass, damping and stiffness matrices. However, when dealing with the internal nonlinear forces $\mathbf{V}^T\mathbf{g_{nl}}(\mathbf{Vq})$, the physical displacement field $\mathbf{u} \approx \mathbf{Vq}$ should be recovered in order to evaluate the forces in the physical space of all degrees of freedom with a FE solver. This solution is intrusive and computationally expensive. Therefore an explicit formulation of the nonlinear forces depending only on the generalized coordinates should be preferred, which is the topic of section 3.2.

3.1 Enriching the Linear Basis with Dual Modes

When structures are undergoing large displacements and are subjected to geometric nonlinearities, it is necessary to include in the reduction basis modes that contain information on the nonlinear coupling between the modes of the structure such as POD modes, modal derivatives or dual modes. In this paper we focus on the dual mode approach to enrich the projection basis. The determination of the dual modes was proposed in [3–5]. The dual modes are deduced from static nonlinear computations with external loads resulting from linear combinations of modes shapes:

$$\mathbf{f}_k = \mathbf{K}(\Omega)\big(\pm\alpha_1^k\boldsymbol{\phi}_1^{\Omega} \pm \alpha_2^k\boldsymbol{\phi}_2^{\Omega}\cdots\pm\alpha_n^k\boldsymbol{\phi}_n^{\Omega}\big), \tag{7}$$

with the weighting coefficients α_i^k and the number of modes n in the reduction basis. Relevant modes are then selected from a Singular Value Decomposition (SVD) and a strain energy criteria. The definition of the forces $\mathbf{f}_k$ is based on the linear normal modes to span a large variety of loadings. The linear combination of linear normal modes is multiplied by the stiffness matrix $\mathbf{K}(\Omega)$ for homogeneity reasons, but also to control the range of the resulting displacements. Indeed, the latter should be large enough to be in the nonlinear range but not too large to remain realistic regarding the yield stress of the material. If geometric nonlinearities were neglected, the linear displacement obtained with such loads would be the linear combination of modes itself.

The process to determine the dual modes consists first in computing the nonlinear static solutions $\mathbf{u}_k$ resulting from the previously introduced load cases of Eq.(7): $\mathbf{K}(\Omega)\mathbf{u}_k + \mathbf{g_{nl}}(\mathbf{u}_k) = \mathbf{f}_k$. Then, the residual with respect to the initial reduction basis of the first linear normal modes is identified for each solution. This residual $\mathbf{r}_k = \mathbf{u}_k - \boldsymbol{\Phi}^{\Omega}\mathbf{q}_k$ is defined as the difference between the nonlinear solution $\mathbf{u}_k$ corresponding to the prescribed loading $\mathbf{f}_k$ and its approximation on the linear normal mode basis $\boldsymbol{\Phi}^{\Omega}\mathbf{q}_k$. The generalized coordinates $\mathbf{q}_k$ are obtained with a least squares approximation using the pseudo-inverse of the basis $\boldsymbol{\Phi}^{\Omega}$: $\mathbf{q}_k = (\boldsymbol{\Phi}^{\Omega T}\boldsymbol{\Phi}^{\Omega})^{-1}\boldsymbol{\Phi}^{\Omega T}\mathbf{u}_k$. The residuals represent the nonlinear information that is missing in the linear basis. All the residual vectors $\mathbf{r}_k$ are gathered in a matrix, from which a SVD is performed. The main singular vectors associated with the largest singular values are extracted, as well as those satisfying the highest linearized strain energy $\mathscr{E}_i$ defined by:

$$\mathscr{E}_i = \sum_{k=1}^{N_L}\left(\frac{\mathbf{d}_i^T\mathbf{r}_k}{\mathbf{d}_i^T\mathbf{d}_i}\right)^2\mathbf{d}_i^T\mathbf{K}(\Omega)\mathbf{d}_i, \tag{8}$$

with N_L the number of load cases defined in Eq.(7) and $\mathbf{d}_i$ the modes obtained by SVD.

The new reduction basis is therefore the concatenation of the first linear normal modes and the dual modes determined with the previous method: $\mathbf{V} = [\boldsymbol{\Phi}^{\Omega}, \mathbf{D}]$ with $\boldsymbol{\Phi}^{\Omega} = (\boldsymbol{\phi}_i^{\Omega})_{i\in[1,n]}$ and $\mathbf{D} = (\mathbf{d}_i)_{i\in[1,m]}$ such that each $\mathbf{d}_i$ is one of the selected singular vector. Therefore, the reduction basis contains only the first n linear normal modes plus possibly the m dual modes. For the sake of simplicity, n will denote in the following the length of the reduction basis, whether it contains the dual modes or not. The last step to build the ROM is to determine the projected nonlinear forces as an explicit expression of the generalized coordinates.

3.2 Determination of the Nonlinear Coefficients

The projection of the geometrical nonlinear forces in Eq.(4) $\mathbf{V}^T\mathbf{g_{nl}}(\mathbf{Vq})$ does not provide a direct dependency on the generalized coordinates. Instead, the physical displacements $\mathbf{u} \approx \mathbf{Vq}$ should be first rebuilt in the physical space of all the degrees of freedom to evaluate the nonlinear forces with the FE solver, which are finally projected again in the reduced space. This induces a

back-and-forth process between the reduced and the full-order model that is not efficient since many calls to the external full-order FE solver are required. The frame of the study is finite deformations (small strain, large displacements, large rotations) and Saint Venant-Kirchhoff constitutive model. In this case, the nonlinear internal forces are cubic with respect to the degrees of freedom. Consequently, it is assumed that the projected nonlinear forces could be approximated by a third-order polynomial of the generalized coordinates $\mathbf{q}$, such that its k^{th} component writes:

$$\widetilde{g}_{nl}^{k}(\mathbf{q}) \approx \sum_{i=1}^{n}\sum_{j=i}^{n}\beta_{ij}^{k}q_i q_j + \sum_{i=1}^{n}\sum_{j=i}^{n}\sum_{m=j}^{n}\gamma_{ijm}^{k}q_i q_j q_m, \qquad (9)$$

with β_{ij}^{k} and γ_{ijm}^{k} the polynomial coefficients that should be identified. For that purpose, two non-intrusive methods relying on nonlinear static computations are recurrent in the literature. On one side the STEP (STiffness Evaluation Procedure) [18] relies on a set of computations performed with prescribed displacements, defined as well-chosen linear combinations of the eigenmodes. Nonlinear internal forces are extracted from these computations and used to evaluate the nonlinear coefficients of the polynomial. Although this method is efficient for 2D structures, specific corrections are needed for 3D structures [19, 20] since perturbations are introduced by possible conflicts between the natural volumetric dilatation/compression of the structure and the one imposed by the prescribed displacement. The second method, which is not sensitive to these artifacts, is the *Implicit Condensation* (IC) [12] and its *Expansion* (ICE) [13]. In this method, nonlinear static computations are performed with prescribed loads, whose distributions are related to the linear normal modes shapes. The nonlinear static solutions as well as the nonlinear internal forces are computed. The generalized coordinates associated with the static solutions are extracted with a pseudo-inverse from the equation $\mathbf{u} \approx \mathbf{V}\mathbf{q}$ and the nonlinear internal forces are projected on the reduction basis and identified with the expression Eq.(9) using a least-squares approximation. In the literature, the IC determination of nonlinear coefficients is used with reduction bases containing only the first linear normal modes. When dual modes are added to the structure, the STEP method is usually preferred to determine the coefficients for simplicity. However, for the reasons detailed previously, the STEP method for 3D cases is not adapted. The originality in this paper is to apply the IC method with a reduction basis containing both linear normal modes and dual modes. In this case, the dual modes are not used in the combinations in Eq.(7) for the construction of the imposed loads, but they have a contribution in the resulting nonlinear static solutions. Thus, both their associated generalized coordinates and those associated to the linear normal modes are extracted by least-squares approximation in the equation $\mathbf{u} \approx \mathbf{V}\mathbf{q}$. Then the entire reduction basis containing the linear normal modes and the dual modes is used for the determination of the polynomial coefficients of the nonlinear internal forces. Nevertheless, the condition number of the system to solve is high since both quadratic and cubic monomials of the generalized coordinates are involved. Besides, many of these nonlinear coefficients (unknowns) are null for some cases (due to symmetry reasons). Considering the previous remarks, the Lasso regression [21] is particularly adapted and could be preferred to the usual least-squares approximation.

Originally reserved to linear normal modes, the IC method is used in this paper for a reduction basis containing both linear normal modes and dual modes. Furthermore, the classical ICE method is considered to compare both approaches. The next section provides more details on the ICE method.

3.3 Implicit Condensation and Expansion for Linear Normal Modes Bases

The ICE method is an extension of the *Implicit Condensation*: the reduced dynamics of the structure is computed for the first linear normal modes only and the total displacement is expanded in post-processing to include in-plane (membrane) effects. The expansion step is based on a static reconstruction using additional modes $\mathbf{\Psi}$ and generalized coordinates $\boldsymbol{\eta}$. The displacement is finally defined with the ICE method as:

$$\mathbf{u}_{\text{ICE}} = \mathbf{\Phi}^{\Omega}\mathbf{q} + \mathbf{\Psi}\boldsymbol{\eta}, \qquad (10)$$

The generalized coordinates $\mathbf{q}$ are computed as the solution of the reduced equation of the dynamics Eq.(6) with $\mathbf{V} = \mathbf{\Phi}^{\Omega}$ including only the first linear modes. On the contrary, the generalized coordinates $\boldsymbol{\eta}$ associated to the modes $\mathbf{\Psi}$ are explicitly defined as quadratic combinations of the generalized coordinates $\mathbf{q}$:

$$\boldsymbol{\eta} = [q_1^2 \quad q_1q_2 \quad q_1q_n \quad \cdots \quad q_2q_3 \quad q_n^2]^T. \qquad (11)$$

The reconstruction modes $\mathbf{\Psi}$ are identified from Eq.(10) using the set of precomputed nonlinear static solutions $\mathbf{u}_k$. Originally the ICE method was used for von Kármán beams and plates for which the modes $\mathbf{\Psi}$ correspond to the membrane displacements.

The previous section presented theoretical aspects of the dynamics of the structure and the construction of the reduced-order model. The next two sections are dedicated to numerical applications with 3D finite element models. Two different applications are presented in this paper: the first one analyses a cantilever beam-like structure in order to present and validate the proposed method. Then, the second one presents a preliminary study of an industrial application of a UHBR new generation turbofan blade.

4. APPLICATION TO 3D CANTILEVER BEAM-LIKE STRUCTURES

The first application is a beam-like structure discretized with 3D HEX20 finite elements (360 elements, 2181 nodes). The length of the beam is equal to 4 m, its thickness 7.10^{-2} m and its width 21.10^{-2} m. The Young's modulus is equal to 100 GPa, the density 4400 kg.m^{-3} and the Poisson's ratio is equal to 0.3. Reference full-order computations are performed using the FE solver *Code_Aster*.

4.1 Vibrations of the Beam Without Rotation

We first investigate the case of a cantilever beam without rotation. The 3 first linear normal modes of the structure are shown in Fig.1. Their frequencies are respectively 3.38 Hz, 10.11 Hz and 21.17 Hz.

The linear normal modes basis is enriched with dual modes according to the process presented in section 3.1. A set of loads are applied to the beam; the residuals of the nonlinear static

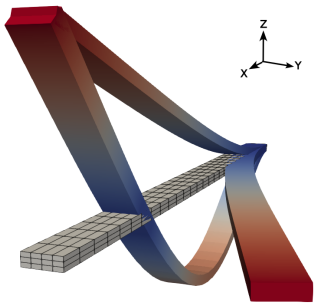

FIGURE 1: VISUALIZATION OF THE FIRST 3 LINEAR NORMAL MODES OF THE BEAM AT 0 RPM. THE MESH IS THE INITIAL GEOMETRY.

solutions are extracted and a SVD is performed on the matrix gathering the residuals. Figure 2 shows the first singular values of the SVD as well as the linearized strain energies of the SVD modes. On this graph, we notice that the first two SVD modes with the largest linearized strain energies correspond also to those with the highest singular values.

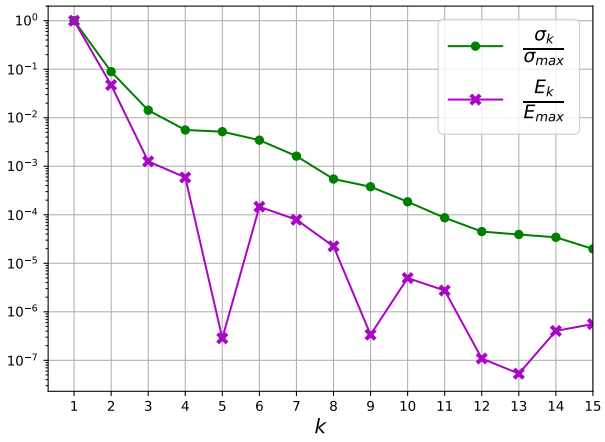

FIGURE 2: NORMALIZED SINGULAR VALUES (GREEN) AND LINEARIZED STRAIN ENERGY (PURPLE) OF THE MODES OBTAINED BY THE SVD OF THE MATRIX OF RESIDUALS.

Those two modes lead to sufficient precision and are therefore selected as dual modes to enhance the linear normal modes basis. The shape of those dual modes is illustrated in Fig.3 showing that those modes are characterized by a purely axial deformation. Indeed, the first linear normal modes correspond to bending movements, triggering membrane displacements due to geometric nonlinearity.

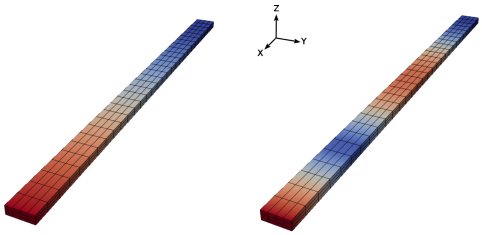

FIGURE 3: DUAL MODES ADDED TO THE LINEAR BASIS.

First, a static external load of amplitude 30000 N is applied vertically at the tip of the beam. Figure 4 presents a comparison of the static deflections between the nonlinear FOM and the ROMs. For such a case, the reduced-order models ICE and IC with dual modes (later referred to as ICDual) are superimposed with the nonlinear FOM solution. Both the static nonlinear solutions obtained with the ICE method and the ICDual method capture the nonlinear behavior of the structure. Nevertheless, the nonlinear static solution of the ICE method matches with the FOM solution after the expansion postprocessing step, while with the ICDual approach, the nonlinear solution is captured directly from the resolution of the reduced system.

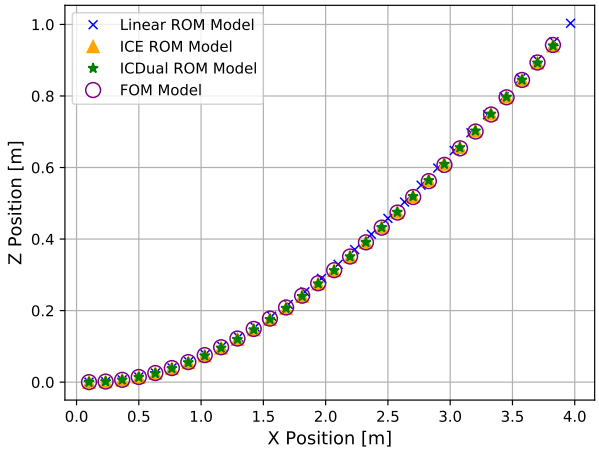

FIGURE 4: COMPARISON OF THE NONLINEAR STATIC SOLUTION BETWEEN THE NONLINEAR FOM AND THE DIFFERENT ROMS.

A dynamic sinusoidal load is then applied vertically at the tip of the beam, with an amplitude of 2500 N, and a forcing frequency equal to the one of the first linear normal mode (3.38 Hz). The time integration is performed using an HHT-α scheme with $\alpha_{\text{HHT}} = 0.05$ and a time step of 2.10^{-3}s. Besides, a Rayleigh viscous damping is considered: $\mathbf{C} = 2\xi\omega_0\mathbf{M}$ with a damping ratio $\xi = 0.05$ and ω_0 the pulsation of the first linear normal mode. Fig.5 depicts the nonlinear displacement of the FOM over one period and Figure 6 represents the axial and vertical temporal displacements of the node in the center of the tip of the beam.

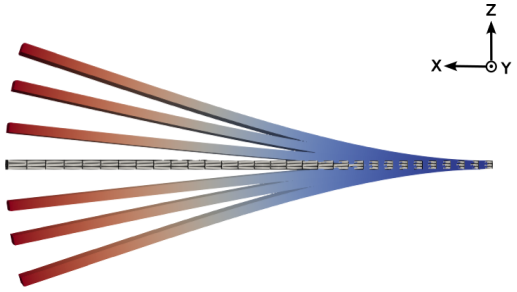

FIGURE 5: NONLINEAR FOM DISPLACEMENTS OVER A PERIOD.

For such levels of deformation, the geometric nonlinearity of the structure is significant. Figure 7 compares the maximal displacements in periodic regime of the FOM solution, the linear ROM solution and the solutions obtained with the reduced-order

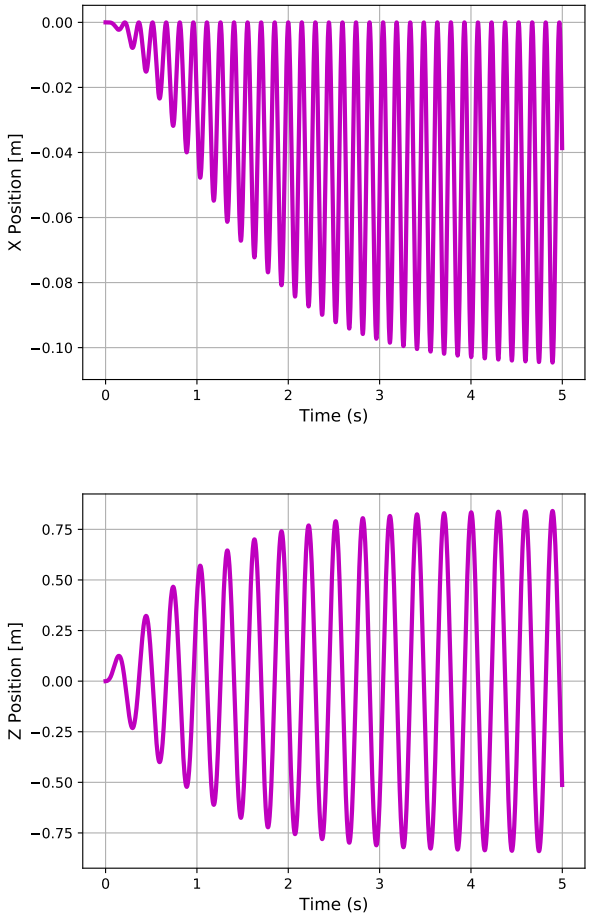

FIGURE 6: TEMPORAL AXIAL AND VERTICAL DISPLACEMENTS OF THE TIP OF THE BEAM.

models ICE and ICDual. The linear ROM solution does not capture at all the axial shortening of the beam resulting from the nonlinearity. Such axial shortening is captured by the *Expansion* step of the ICE method but slightly differs from the FOM solution, which was not the case for the previous test case with a static load. This difference results from the *Expansion* step of the ICE method which is based on a static reconstruction of the solution from the bending dynamics, but the membrane dynamics itself is not solved in the reduced equation of the dynamics. On the contrary, the addition of dual modes to the reduction basis leads to the resolution of the dynamics in traction-compression directly in the reduced equation of the dynamics Eq.(6). Therefore, no reconstruction is needed and the dynamics is more accurately captured.

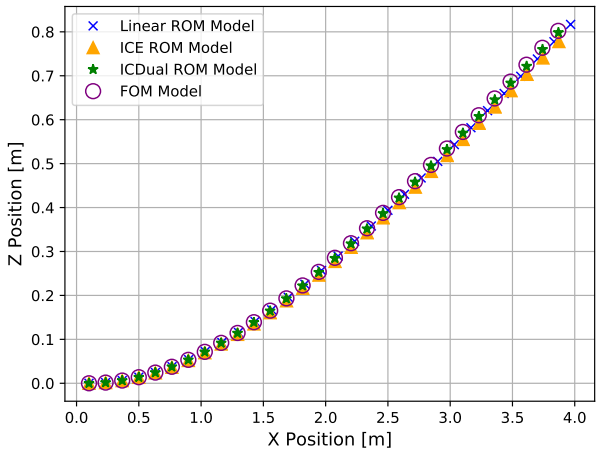

FIGURE 7: COMPARISON OF THE MAXIMAL DISPLACEMENTS IN PERIODIC REGIME BETWEEN THE FOM AND THE DIFFERENT ROM SOLUTIONS. THE BEAM IS SUBJECTED TO A VERTICAL SINUSOIDAL LOAD AT THE TIP OF AMPLITUDE 2500 N AND FREQUENCY 3.38 HZ.

4.2 Rotation at Constant Rotating Velocity

In this section, the beam is shifted of 10 cm from the vertical axis and rotates around the latter at a constant speed of 500 rpm. Centrifugal effects arise and the equilibrium position of the structure is the prestressed position due to the centrifugal forces, around which the linear normal modes are computed. The shape of the 3 linear normal modes are very similar to those without rotation (see Fig.1) but their respective modal frequencies become 9.67 Hz, 10.86 Hz and 30.22 Hz. Then the process of determining the dual modes is applied. Fig.8 represents the singular values and the linearized strain energies of the SVD modes. The dual modes selected are the first two SVD modes, which have a similar shape as those of the case without rotation illustrated in Fig.3.

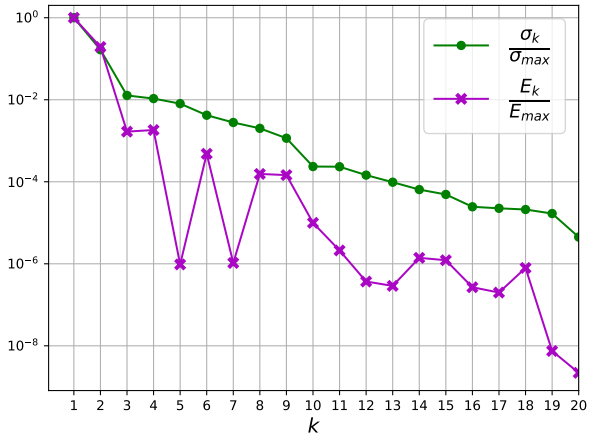

FIGURE 8: NORMALIZED SINGULAR VALUES (GREEN) AND LINEARIZED STRAIN ENERGY (PURPLE) OF THE SVD MODES OF THE BEAM IN ROTATION AT 500 RPM.

Similarly to the non-rotating analysis of the beam, a static

load is applied vertically at the tip. In order to reach a comparable level of displacement, the applied load amplitude (210000 N) is seven times larger than in the case without rotation. Figure 9 compares the nonlinear FOM static deflection with the ROM solutions. As in the non-rotating case, the linear ROM solution does not capture the bending/membrane displacements coupling due to geometric nonlinearity. Both the ICE and ICDual models capture the nonlinear coupling leading to axial shortening. Nevertheless, due to the axial centrifugal forces and the vertical loading at the tip, the curvature of the beam is larger than the case without rotation. Such curvature is not perfectly captured by the ROMs. Regarding the position of the tip, the ICDual solution matches with the FOM solution, while the ICE solution underestimates the vertical displacement.

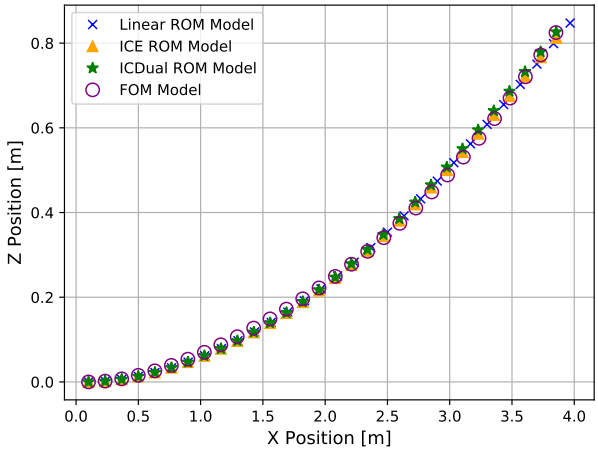

FIGURE 9: COMPARISON OF THE STATIC DEFLECTIONS BETWEEN THE FOM AND THE DIFFERENT ROMS. THE BEAM IS IN ROTATION AT 500 RPM SUBJECT TO A VERTICAL STATIC LOAD AT THE TIP OF 210000 N.

To echo the test case of the beam without rotation, this second study deals with a dynamic loading applied vertically at the tip. The frequency of excitation is the one of the first linear normal mode in rotation (9.67 Hz) and its amplitude is 7350 N, about three times the load of the non-rotating case in order to reach a similar magnitude of displacements. The same integration scheme as for the case without rotation is used but the time step is reduced by half. The Rayleigh damping is kept unchanged.

The nonlinear solutions with the reduced-order models ICE and ICDual are also computed. Figure 10 compares the maximal amplitudes in periodic regime between the FOM, the ICE, the ICDual and the linear ROM solutions, under the above-mentioned dynamic load. While the solution with dual modes has a negligible error with respect to the nonlinear FOM solution, the ICE method slightly underestimates the amplitude of displacement; more linear normal modes would be needed in the reduction basis for the ICE method.

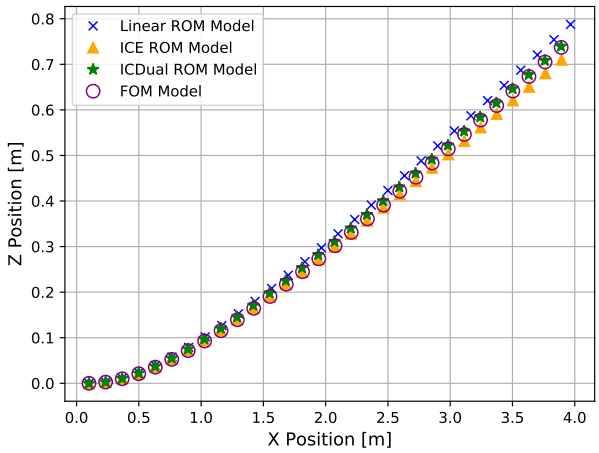

FIGURE 10: COMPARISON OF THE MAXIMAL DISPLACEMENT IN PERIODIC REGIME BETWEEN THE FOM AND THE DIFFERENT ROM SOLUTIONS. THE BEAM IS SUBJECT TO A VERTICAL SINUSOIDAL LOAD AT THE TIP, OF AMPLITUDE 7350 N AND FREQUENCY 9.67 HZ.

5. APPLICATION TO A FAN BLADE

In this section, we consider a complex 3D structure of a fan blade representative of a UHBR turbofan. The objective is to investigate the accuracy and robustness of the structural reduced order model for such structures with representative aerodynamic loads.

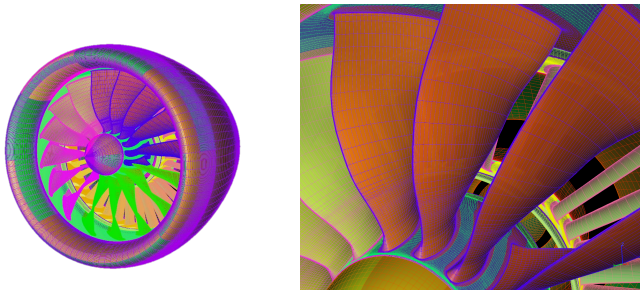

FIGURE 11: VISUALIZATION OF THE FULL ENGINE MODEL AND THE FAN BLADES.

Figure 11 illustrates the full engine configuration (on the left) and the fan blade of interest (on the right). In the present work, we consider a single fan blade (all blades being the same). The original blade structural model has been adapted to enable a dynamic analysis restricted to a single fan blade: for that purpose, the blade root was removed and replaced by a clamped boundary condition. The Young's modulus is equal to 110 GPa, the density 4500 kg.m^{-3} and the Poisson's ratio is equal to 0.318. The blade is discretized in 66640 HEX8 finite elements, with 6 elements in the blade thickness. The structural mesh of the blade is shown in Fig.12 from two different angles of view.

The structure is in rotation around a fixed axis, centrifugal effects are present and the dynamics of the structure is studied around the prestressed position. The linear normal modes shapes of the structure and their associated modal frequencies are modified by the rotation speed since they are computed relative to the

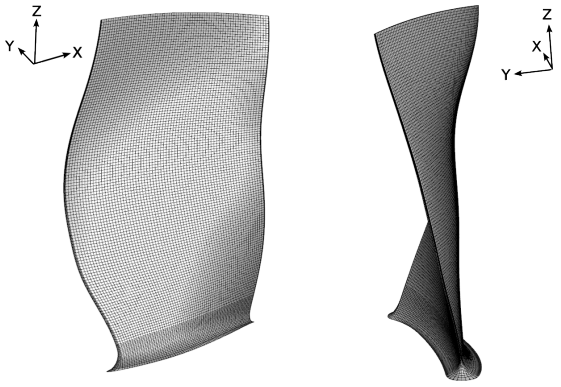

FIGURE 12: MESH OF THE BLADE.

prestressed position. Fig.13 is a Campbell diagram showing the evolution of the frequencies of the first three linear normal modes with respect to the rotation speed.

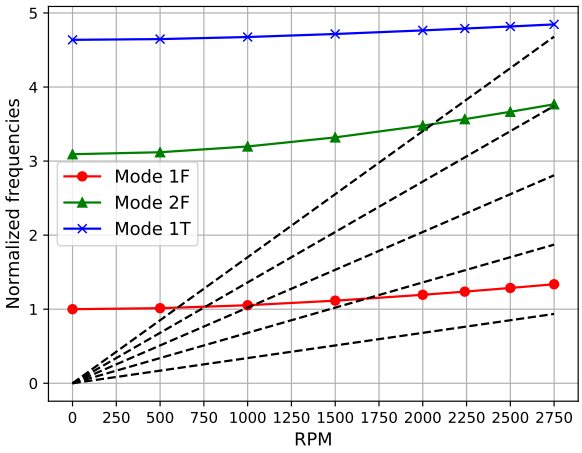

FIGURE 13: CAMPBELL OF THE BLADE FOR THE FIRST 3 STRUCTURAL MODES.

The first linear normal modes are respectively the first bending mode (named 1F), the second bending mode (2F) and the first torsion mode (1T). Figure 14 presents the modes 1F, 2F and 1T at the rotation speed of 2750 rpm. It is noticed on the Campbell diagram, that at 2750 rpm, the modes 2F and 1T are close to multiples of the rotation speed. Resonance can therefore be observed at this rotating speed for those modes, which should be avoided.

In what follows, the rotating speed considered is 2750 rpm. The centrifugal effects lead to an untwisting of the blade. First, a static load will be applied to the structure, then a dynamic forcing.

5.1 Nonlinear Response under a Static Load

In this section, a static load is applied to the structure. The load is based on the shape of the first linear normal mode at 2750 rpm as follows:

$$\mathbf{f_{ext}} = -15h\mathbf{K}(\Omega)\frac{\boldsymbol{\phi}_1^{2750}}{\max|\boldsymbol{\phi}_1^{2750}|}, \qquad (12)$$

with h the average thickness of the blade tip. For such a load shape, the maximal amplitude of the linear solution is 15 times

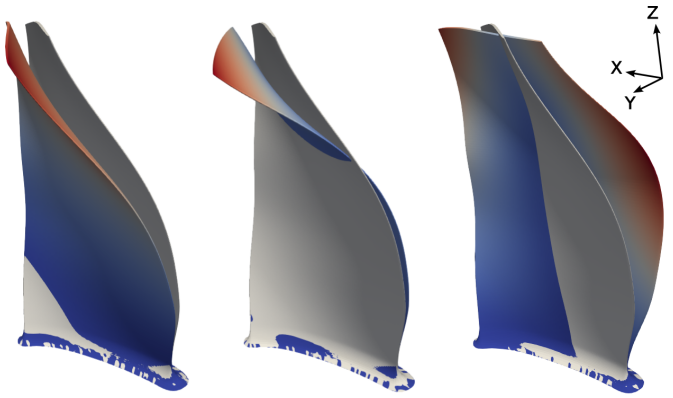

FIGURE 14: FIRST 3 LINEAR NORMAL MODES (1F, 2F AND 1T) OF THE BLADE AT 2750 RPM.

the thickness of the blade tip. The linear and ICE ROMs are both built using the first 3 linear normal modes and the first dual mode is added for the ICDual ROM. Figure 15 represents the solution obtained under the static load of Eq.(12) and Fig.16 under its opposite.

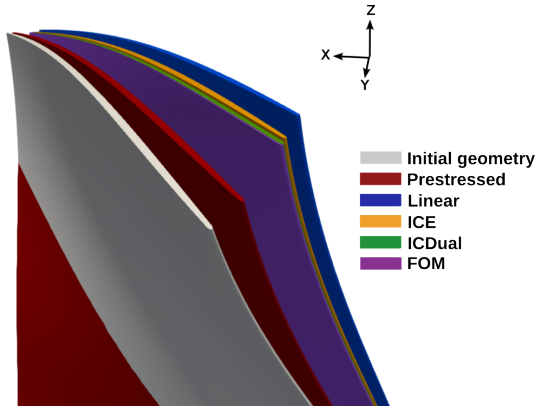

FIGURE 15: COMPARISON BETWEEN THE FOM AND THE ROM SOLUTIONS UNDER THE STATIC LOAD (12).

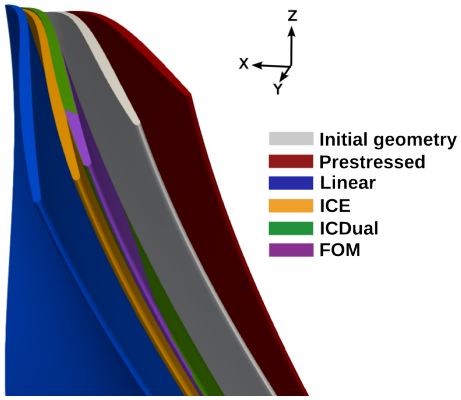

FIGURE 16: COMPARISON BETWEEN THE FOM AND THE ROM SOLUTIONS UNDER THE OPPOSITE OF THE STATIC LOAD (12).

The geometrical nonlinearity is significant for such ampli-

tudes. The nonlinear ICDual solution matches perfectly with the FOM solution but the ICE solution presents a slight deviation at the tip and the linear ROM solution overestimates the static displacement.

5.2 Nonlinear Response under a Dynamic Load

The previous section compared the nonlinear displacement between the linear and the nonlinear solutions under a static load. The purpose of this section is to compare the FOM solution to the linear and nonlinear reduced solutions under a dynamic load. Like the static load, the dynamic load is based on the mode shape of the normal mode 1F with a sinusoidal forcing at its resonance frequency:

$$\mathbf{f_{ext}} = 1.5h\mathbf{K}(\Omega)\left(\frac{\boldsymbol{\phi}_1^{2750}}{\max|\boldsymbol{\phi}_1^{2750}|}\right)\sin(\omega_0^{2750}t), \qquad (13)$$

with ω_0^{2750} the pulsation of the first linear normal at 2750 rpm. A Rayleigh damping is considered: $\mathbf{C} = 2\xi\omega_0^{2750}\mathbf{M}$ with $\xi = 0.05$.

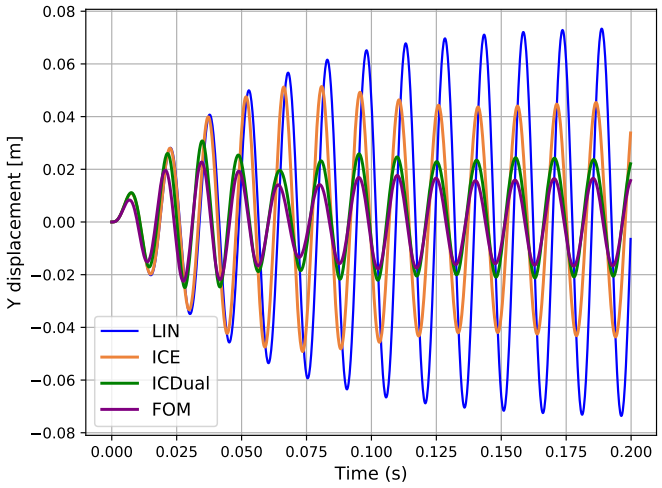

FIGURE 17: TIME RESPONSE OF THE TIP TRAILING EDGE ALONG THE Y DIRECTION.

Figure 17 represents the time evolution of the tip leading edge of the blade along the Y direction. As expected, the levels of vibration of the nonlinear models are much lower than the linear one. There is a significant difference between the ICE and ICDual ROMs, the latter depicting lower levels of vibrations that are closer to those obtained with the FOM computation. The computation of the FOM dynamic solution takes about 10 hours using parallel computing and a significant memory while the resolution with the ROMs takes less than 10 seconds on a single processor. The precision of both the ICE and ICDual models can be improved with a more accurate choice of external loads, closer to the targeted dynamic displacement. Indeed, during the construction of the model, the nonlinear static solutions obtained under the loads $\mathbf{f}_k$ are approximated in the reduction basis. Therefore, the precision of the ICE method is strongly dependent on the amplitude of the external loads which is less the case with the ICDual method due to the richer reduction basis.

5.3 Aerodynamic Forces

In the previous sections, the external forces applied to the blade were arbitrary loads. Ongoing work is to impose aerodynamic forces resulting from unsteady CFD computations of the entire engine fan. Figure 18 illustrates the components of the aerodynamic forces in the 3 spatial directions resulting from a steady CFD computation. The objective is to assess the behavior of the ROM under distributed loads, first in a static case under the aerodynamic forces resulting from the steady CFD computation, then for dynamic analyses under unsteady aerodynamic loads. Finally, the aim is to carry out an aeroelastic computation using a partitioned approach by coupling the CFD solver with the ROM.

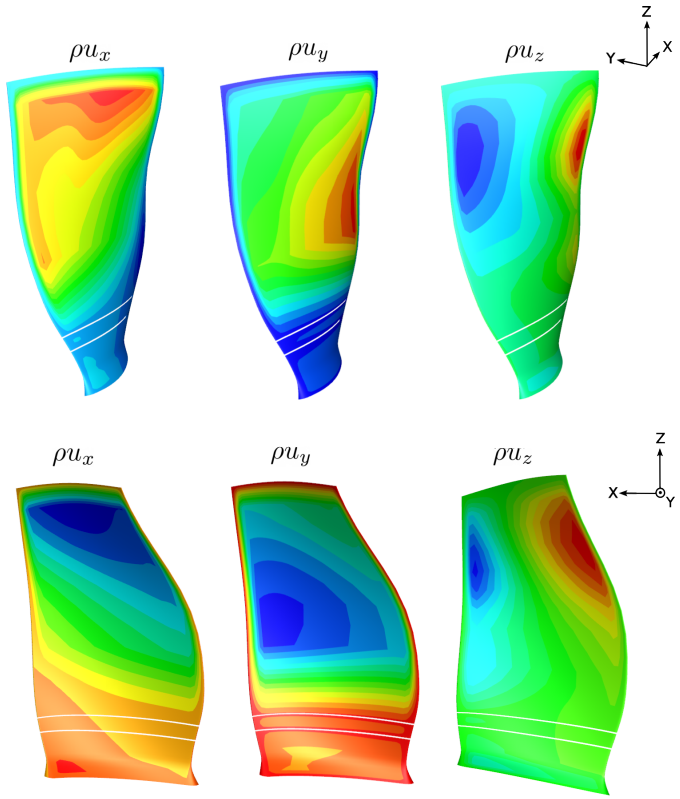

FIGURE 18: STEADY AERODYNAMIC FORCES ON THE SUCTION SIDE (TOP) AND THE PRESSURE SIDE (BOTTOM) OF THE BLADE.

6. CONCLUSION

In this paper, a reduced-order model for 3D structures subject to geometric nonlinearities is developed based on dual modes and *Implicit Condensation*. This ROM is compared to the usual ICE method in the cases of a cantilever beam in rotation and a fan blade. The results obtained show that the proposed approach better captures the nonlinear geometric behavior. The application to a fan blade under aerodynamic loading is introduced and preliminary results are obtained under external forcing.

ACKNOWLEDGMENTS

This work is co-financed by the research and innovation program of the European Union Horizon 2020 in the frame of the project Clean Sky 2 ADEC and the platform LPA-IADP

REFERENCES

[1] Nelson, R. "Simplified Calculation of Eigenvector Derivatives." *AIAA Journal* Vol. 14 No. 9 (1976): pp. 1201–1205. DOI https://doi.org/10.2514/3.7211.

[2] Slaats, P.M.A., de Jongh, J. and Sauren, A.A.H.J. "Model Reduction Tools for Nonlinear Structural Dynamics." *Computers & Structures* Vol. 54 No. 6 (1995): pp. 1155–1171. DOI https://doi.org/10.1016/0045-7949(94)00389-K.

[3] Kim, K., Radu, A.G., Wang, X.Q. and Mignolet, M.P. "Nonlinear Reduced Order Modeling of Isotropic and Functionally Graded Plates." *International Journal of Non-Linear Mechanics* Vol. 49 (2013): pp. 100–110. DOI https://doi.org/10.1016/j.ijnonlinmec.2012.07.008.

[4] Mignolet, M.P., Przekop, A., Rizzi, S.A. and Spottswood, S.M. "A Review of Indirect/Non-intrusive Reduced Order Modeling of Nonlinear Geometric Structures." *Journal of Sound and Vibration* Vol. 332 No. 10 (2013): pp. 2437–2460. DOI https://doi.org/10.1016/j.jsv.2012.10.017.

[5] Wang, X. Q., Khanna, V., Kim, K. and Mignolet, M.P. "Nonlinear Reduced-Order Modeling of Flat Cantilevered Structures: Identification Challenges and Remedies." *Journal of Aerospace Engineering* Vol. 34 No. 6 (2021): p. 04021085. DOI 10.1061/(ASCE)AS.1943-5525.0001324.

[6] Vizzaccaro, A., Opreni, A., Salles, L., Frangi, A. and Touzé, C. "High Order Direct Parametrisation of Invariant Manifolds for Model Order Reduction of Finite Element Structures: Application to Large Amplitude Vibrations and Uncovering of a Folding Point." *Nonlinear Dynamics* Vol. 110 No. 1 (2022): pp. 525–571. DOI https://doi.org/10.1007/s11071-022-07651-9.

[7] Haller, G. and Ponsioen, S. "Nonlinear Normal Modes and Spectral Submanifolds: Existence, Uniqueness and use in Model Reduction." *Nonlinear Dynamics* Vol. 86 No. 3 (2016): pp. 1493–1534. DOI https://doi.org/10.1007/s11071-016-2974-z.

[8] Chaturantabut, S. and Sorensen, D.C. "Nonlinear Model Reduction via Discrete Empirical Interpolation." *SIAM Journal on Scientific Computing* Vol. 32 No. 5 (2010): pp. 2737–2764. DOI 10.1137/090766498.

[9] Feeny, B.F. and Kappagantu, R. "On the Physical Interpretation of Proper Orthogonal Modes in Vibrations." *Journal of Sound and Vibration* Vol. 211 No. 4 (1998): pp. 607–616. DOI https://doi.org/10.1006/jsvi.1997.1386.

[10] Kerschen, G. and Golinval, J.C. "Physical Interpretation of the Proper Orthogonal Modes using the Singular Value Decomposition." *Journal of Sound and Vibration* Vol. 249 No. 5 (2001): pp. 849–865. DOI https://doi.org/10.1006/jsvi.2001.3930.

[11] Liang, Y.C. et al. "Proper Orthogonal Decomposition and its Applications." *Journal of Sound and Vibration* Vol. 252 No. 3 (2002). DOI https://doi.org/10.1006/jsvi.2001.4041.

[12] McEwan, M.I., Wright, J.R., Cooper, J.E. and Leung, A.Y.T. "A Combined Modal/Finite Element Analysis Technique for the Dynamic Response of a Non-Linear Beam to Harmonic Excitation." *Journal of Sound and Vibration* Vol. 243 (2001): pp. 601–624. DOI https://doi.org/10.1006/jsvi.2000.3434.

[13] Hollkamp, J.J. and Gordon, R.W. "Reduced-Order Models for Nonlinear Response Prediction: Implicit Condensation and Expansion." *Journal of Sound and Vibration* Vol. 318 No. 4-5 (2008): pp. 1139–1153. DOI https://doi.org/10.1016/j.jsv.2008.04.035.

[14] Nicolaidou, E., Hill, T.L. and Neild, S.A. "Indirect Reduced-Order Modelling: using Nonlinear Manifolds to Conserve Kinetic Energy." *Proc. R. Soc. A.* No. 476 (2020). DOI http://doi.org/10.1098/rspa.2020.0589.

[15] Nicolaidou, E., Hill, T.L. and Neild, S.A. "Nonlinear Mapping of Non-Conservative Forces for Reduced-Order Modelling." *Proc. R. Soc. A* No. 478 (2022): p. 20220522. DOI https://doi.org/10.1098/rspa.2022.0522.

[16] Flament, T., Deü, J.-F., Placzek, A., Balmaseda, M. and Tran, D.-M. "Reduced-Order Model for Large Amplitude Vibrations of Flexible Structures Coupled with a Fluid Flow." *ECCOMAS*. 2022. Oslo, Norway.

[17] Thomas, O., Sénéchal, A. and Deü, J.-F. "Hardening/Softening Behavior and Reduced Order Modeling of Nonlinear Vibrations of Rotating Cantilever Beams." *Nonlinear Dynamics* Vol. 2 No. 86 (2016): pp. 1293–1318. DOI https://doi.org/10.1007/s11071-016-2965-0.

[18] Muravyov, A.A. and Rizzi, S.A. "Determination of Nonlinear Stiffness with Application to Random Vibration of Geometrically Nonlinear Structures." *Computers & Structures* Vol. 81 (2003-07): pp. 1513–1523. DOI https://doi.org/10.1016/S0045-7949(03)00145-7.

[19] Balmaseda, M., Jacquet-Richardet, G., Placzek, A. and Tran, D.-M. "Reduced Order Models for Nonlinear Dynamic Analysis With Application to a Fan Blade." *Journal of Engineering for Gas Turbine and Power* Vol. 142 No. 4 (2020): p. 041002. DOI https://doi.org/10.1115/1.4044805.

[20] Vizzaccaro, A., Givois, A., Longobardi, P., Shen, Y., Deü, J.-F., Salles, L., Touzé, C. and Thomas, O. "Non-intrusive Reduced Order Modelling for the Dynamics of Geometrically Nonlinear Flat Structures using Three-Dimensional Finite Elements." *Computational Mechanics* Vol. 66 No. 6 (2020): pp. 1293–1319. DOI https://doi.org/10.1007/s00466-020-01902-5.

[21] Tibshirani, R. "Regression Shrinkage and Selection via the Lasso." *Journal of the Royal Statistical Society: Series B (Methodological)* Vol. 58 No. 1 (1996): pp. 267–288.

[22] S. Heib, L. Cambier, S. Plot. "The Onera elsA CFD Software: input Research and Feedback from Industry." *Mechanics & Industry, EDP Sciences* Vol. 14 No. 3 (2013): pp. 159–174. DOI https://doi.org/10.1051/meca/2013056.